Effects of altering histone posttranslational modifications on mitotic chromosome structure and mechanics

Ronald Biggs[a], Patrick Z. Liu[a], Andrew D. Stephens[a], and John F. Marko[a,b,*]
[a]Department of Molecular Biosciences and [b]Department of Physics and Astronomy, Northwestern University, Evanston, IL 60208

ABSTRACT **During cell division, chromatin is compacted into mitotic chromosomes to aid faithful segregation of the genome between two daughter cells. Posttranslational modifications (PTMs) of histones alter compaction of interphase chromatin, but it remains poorly understood how these modifications affect mitotic chromosome stiffness and structure. Using micropipette-based force measurements and epigenetic drugs, we probed the influence of canonical histone PTMs that dictate interphase euchromatin (acetylation) and heterochromatin (methylation) on mitotic chromosome stiffness. By measuring chromosome doubling force (the force required to double chromosome length), we find that histone methylation, but not acetylation, contributes to mitotic structure and stiffness. We discuss our findings in the context of chromatin gel modeling of the large-scale organization of mitotic chromosomes.**

Monitoring Editor
A. Gregory Matera
University of North Carolina

Received: Sep 21, 2018
Revised: Jan 3, 2019
Accepted: Jan 4, 2019

INTRODUCTION

Chromatin structure is important for many different cellular functions. A dramatic change in chromatin structure and organization occurs during the transition from interphase to mitosis as the open, diffuse, compartmentalized, and transcriptionally accessible interphase chromatin becomes compact, rod-like, and transcriptionally repressed in mitosis (Wang and Higgins, 2013; Doenecke, 2014; Oomen and Dekker, 2017). Although most work studying mitotic chromatin rearrangement focuses on large chromatin-organizing complexes like cohesin, condensin, and topoisomerases (Vagnarelli, 2012), mitosis also is associated with characteristic changes to histone posttranslational modifications (PTMs; Wang and Higgins, 2013; Oomen and Dekker, 2017).

Histone PTMs are chemical changes to histones, typically to their tails, some of which are associated with different chromatin structures and densities (Rice and Allis, 2001; Wang and Higgins, 2013). Acetylation, notably of histone 3 lysine 9 (H3K9ac), is associated with euchromatin, which is loosely packed, gene rich, and actively transcribed (Doenecke, 2014). Methylation, notably H3K9me^3 and H3K27me^3, is associated with heterochromatin, which is densely packed and poorly transcribed (Rice and Allis, 2001; Wang and Higgins, 2013; Oomen and Dekker, 2017). Histone PTMs may also intrinsically alter chromatin packing by changing the charge of histones (acetylation) and introducing hydrophobic moieties to histones (methylation; Rice and Allis, 2001; Doenecke, 2014). Recent cryo-EM data have shown that histones are often positioned such that histone tails can physically interact with other nearby histone tails (Bilokapic *et al.*, 2018), possibly enabling the alteration to chromatin structure.

Changes to histone PTMs are known to affect the structure and stiffness of cell nuclei during interphase. Increased euchromatin has been correlated with weaker nuclei (Chalut *et al.*, 2012; Krause *et al.*, 2013; Haase *et al.*, 2016) specifically decreasing the short-extension force response of nuclei, which is governed by chromatin stiffness, and contributes secondarily to long extensions (Stephens *et al.*, 2017). Chromatin stiffness also contributes to nuclear shape (Banigan *et al.*, 2017). Decreased chromatin-based nuclear rigidity caused by increased euchromatin has also been shown to cause abnormal nuclear morphology (Stephens *et al.*, 2018), which is an indicator of different cellular diseases, including cancers (Chow *et al.*, 2012). Increased heterochromatin has been shown to cause stiffer nuclei and

This article was published online ahead of print in MBoC in Press (http://www.molbiolcell.org/cgi/doi/10.1091/mbc.E18-09-0592) on January 9, 2019.

R.B. and J.F.M. conceived and designed the research. R.B., A.D.S., and P.L. conducted experiments. R.B. and P.L. analyzed data. R.B., A.D.S., and J.F.M. wrote, read, and approved the manuscript.

*Address correspondence to: John F. Marko (john-marko@northwestern.edu).

Abbreviations used: ac, acetylation; cryo-EM, cryogenic electron microscopy; H3K#, histone 3 lysine # (amino acid position); HDACi, histone deacetylase inhibitor; HDMi, histone demethylase inhibitor; me, methylation (superscript denotes number of methyl groups); MS, methylstat; PBS, phosphate-buffered saline; PTM, posttranslational modification; SMC2, structural maintenance of chromosomes 2; TSA, trichostatin A; VPA, valproic acid.

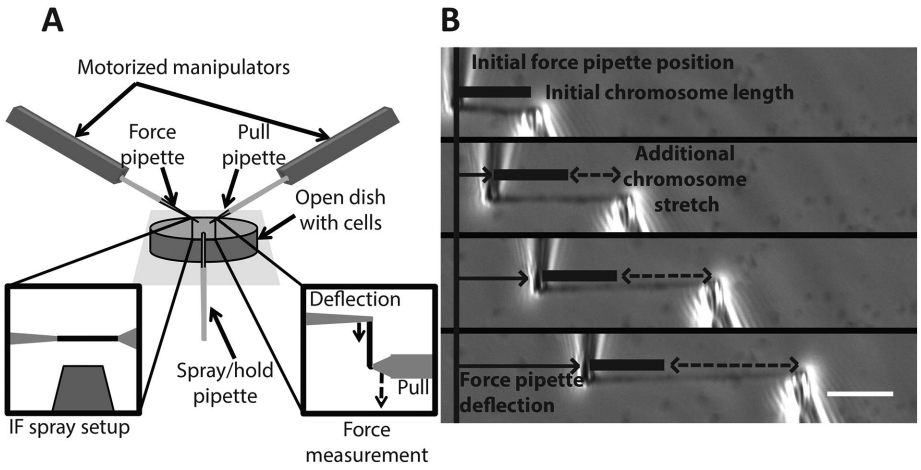

FIGURE 1: Experimental setup for chromosome micromanipulation, force measurement, and image quantification. (A) Schematic of the single captured chromosome experimental setup. Single chromosomes were captured from mitotic HeLa cells in a custom-made well (*Materials and Methods*). Capture was performed after lysing the cell membranes with a PBS–Triton-X solution, where the chromosome was captured from the whole genome chromosome bundle (Supplemental Figure S1). Once captured, the chromosome could be stretched for measurements of the doubling force or sprayed with fluorescent antibodies for immunostaining experiments. (B) An example of an experiment to measure the doubling force of a mitotic chromosome. The force (thin pipette on the left) and pull (larger pipette on the right) pipettes were aligned to be roughly perpendicular to the captured chromosomes. The pull pipette then moved away from the force pipette, stretching the chromosome (dashed line). The stretching of the chromosome would cause the force pipette to deflect (thin, rightward arrow) from its original position (thin, vertical line), which was used to calculate the force on the chromosome for the amount of stretch at that point. Chromosome initial length (thick bar; measured by the distance from the center of the pipettes) and diameter (not shown) measured using a still image in ImageJ.

resistance to abnormal nuclear morphology (Stephens *et al.*, 2017, 2018). Thus, the correlations between chromatin state and histone PTMs with nuclear stiffness and shape indicate underlying connections between histone PTMs and chromatin stiffness.

Some histone PTM changes are associated specifically with mitosis. Bookmarking is the process where some histone PTMs are retained or stabilized during mitosis, which is thought to preserve the cell's transcriptional state through mitosis (Wang and Higgins, 2013; Doenecke, 2014; Oomen and Dekker, 2017). These marks are important for maintaining cellular identity and function. Several histone methyl marks, both euchromatic (e.g., H3K4me^3) and heterochromatic (e.g., H3K9me^3 and H3K27me^3) are possibly increased or maintained in mitosis (Xu *et al.*, 2009; Park *et al.*, 2011). Increased H4K20me^1 has also been associated with loading of condensin, which organizes chromatin in mitosis (Beck *et al.*, 2012). Another hallmark of mitosis is the dramatic reduction in overall histone acetylation (Park *et al.*, 2011; Zhiteneva *et al.*, 2017), which may be important for mitotic compaction or related to the lower transcriptional activity during mitosis (Wang and Higgins, 2013).

Histone PTMs may also intrinsically affect mitotic chromosome organization (Vagnarelli, 2012; Zhiteneva *et al.*, 2017). Recent experiments suggest that nucleosomes reconstituted using core histones from mitotic cells have a greater propensity to aggregate, compared with nucleosomes assembled using core histones from interphase cells (Zhiteneva *et al.*, 2017). This suggests that histone PTMs and their changes in mitosis may intrinsically affect mitotic compaction through nucleosome–nucleosome interactions. Other experiments have shown that DNA forms the underlying connectivity of mitotic chromosomes (Poirier and Marko, 2002; Sun *et al.*, 2011) and condensin in the central axis of mitotic chromosomes is discontiguous (Sun *et al.*, 2018; Walther *et al.*, 2018). Although condensin provides the majority of the stiffness of mitotic chromosomes, it remains unclear how much chromatin–chromatin interactions could contribute to the stiffness of the mitotic chromosome.

To study the effects of altering histone PTMs on mitotic chromosome structure, we measured the doubling forces of captured mitotic chromosomes (Figure 1 and Supplemental Figure S1; the "doubling force" is the force required to double the length of a chromosome, and quantifies chromosome elastic stiffness in a chromosome-length-independent way). To test the hypothesis that alterations to histone PTMs affect the compaction of mitotic chromosomes, we studied the effects of the histone deacetylase inhibitors (HDACis), valproic acid (VPA; Marchion *et al.*, 2005) and trichostatin A (TSA; Yoshida *et al.*, 1990), on the levels of H3K9ac in mitosis and how they affect the stiffness of human mitotic chromosomes. We also tested how the histone demethylase inhibitor (HDMi), methylstat (MS), which is a Jumonji C–specific inhibitor (Luo *et al.*, 2011; a key domain for several demethylases' activity), alters the levels of H3K9me^{2,3} and H3K27me^3 in mitosis, and affects the stiffness of human mitotic chromosomes. Our results show that HDACi treatments increase H3K9ac, but cause no change to the stiffness of mitotic chromosomes, while MS treatment increased canonical heterochromatin marks and the mechanical stiffness of mitotic chromosomes.

RESULTS

HDACis increase H3K9ac on mitotic chromosomes but do not affect their stiffness

To investigate the role of histone PTMs on mitotic chromosome compaction, we studied the effects of histone hyperacetylation. We induced histone hyperacetylation using the HDACis, VPA and TSA. Both VPA and TSA led to an increase in H3K9ac fluorescence intensity in fixed immunofluorescence (IF; Supplemental Figure S2, A and B) and Western blots in interphase cells (Supplemental Figure S2C). Having been able to induce hyperacetylation in interphase, we next tested whether the same treatment would cause histone hyperacetylation in mitosis. In fixed IF experiments of mitotic cells the average ratios of HDACi-treated to untreated H3K9ac acetylation levels were 1.4 ± 0.1 for VPA and 2.3 ± 0.3 for TSA (Figure 2, A and B). In single captured chromosome experiments the average ratios of HDACi to untreated H3K9ac measurements were 1.8 ± 0.2 for VPA and 2.3 ± 0.6 for TSA (Figure 2, C and D). These results indicated that we were able to create hyperacetylated chromatin in mitosis.

Next we tested whether this increase in acetylation would lead to a difference in stiffness for mitotic chromosomes, by measuring the doubling force of mitotic chromosomes extracted from untreated and HDACi-treated cells. Neither VPA nor TSA caused a statistically significant change in doubling force compared with untreated chromosomes (Figure 2E). The average chromosome doubling forces

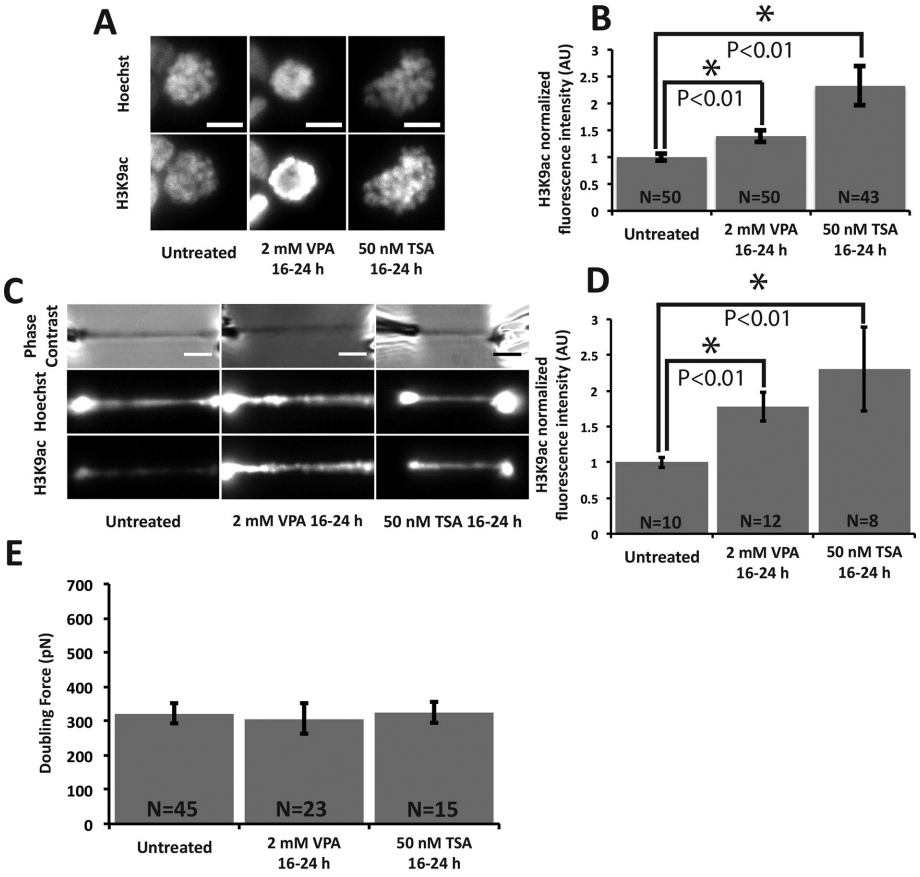

FIGURE 2: HDACis cause increased H3K9ac fluorescence in mitotic fixed cells and captured chromosomes, but have little effect on the stiffness of mitotic chromosomes. (A) Example representative images of levels of H3K9ac fluorescence measurement on fixed mitotic cells. Scale bar = 10 μm. (B) Quantitative data of A. The H3K9ac intensity ratio of untreated to 2 mM VPA 16–24 h treatment was 1.4 ± 0.1 and is statistically significant. The H3K9ac intensity ratio of untreated to 50 nM TSA 16–24 h treatment was 2.3 ± 0.3 and is statistically significant. (C) Example representative images of levels of H3K9ac fluorescence measurements on captured mitotic chromosomes. Scale bar = 5 μm. (D) Quantitative data of C. The H3K9ac intensity ratio of untreated to 2 mM VPA 16–24 h treatment was 1.8 ± 0.2 and is statistically significant. The H3K9ac intensity ratio of untreated to 50 nM TSA 16–24 h treatment was 2.3 ± 0.6 and is statistically significant. (E) Recorded doubling force for mitotic chromosomes from untreated and HDACi-treated cells. The average chromosome doubling forces were 320 ± 30 pN in untreated cells. The average doubling force was 310 ± 40 pN in 2 mM VPA 16–24 h treated cells, statistically insignificantly different compared with untreated cells. The average doubling force was 330 ± 30 pN in 50 nM TSA 16–24 h treated cells, statistically insignificantly different compared with untreated cells. Error bars represent SE. Asterisk in bar graphs represents a statistically significant difference ($p < 0.05$). All p values calculated via t test.

were 320 ± 30 pN in untreated cells, 310 ± 40 pN in VPA-treated cells, and 330 ± 30 pN in TSA-treated cells. The lack of change was not due to changes of initial length or cross-sectional area, as neither changed with HDACi treatments (Supplemental Figure S2, D and E).

Plotting the averaged doubling force against H3K9ac fluorescence for untreated and HDAC inhibited chromosomes, we found that there was no statistically significant correlation between H3K9ac measurements and doubling force in either untreated chromosomes or VPA treatments (Supplemental Figure S2F). We do note that the TSA-treated chromosomes did show a statistically significant correlation between measured H3K9ac level and doubling force, with increasing acetylation leading to lower spring constant; however, when averaged over, there was no net effect of TSA treatment on chromosome spring constant. The correlation may be due to the specific mechanism of HDAC inhibition by TSA (no such correlation was observed for VPA), may reflect differences between specific chromosomes, or simply arise from the sample size being too small for this type of correlation analysis. Apart from this correlation, we concluded that hyperacetylation of histones through HDACi treatment does not affect the overall stiffness of mitotic chromosomes.

Methylstat stiffens mitotic chromosomes and increases fixed-cell histone methylation

Given that there was no overall effect of histone acetylation on chromosome doubling force, we wanted to test how altering histone methylation affects the stiffness of mitotic chromosomes. To induce hypermethylation, we used the HDMi MS, which increased both H3K9me^{2,3} and H3K27me^{3} as assayed via both Western blotting (Supplemental Figure S3, A and B) and fixed-cell IF in interphase cells (Supplemental Figure S3C). Having been able to induce hypermethylation in interphase, we next tested whether the same treatment would cause histone hypermethylation in mitosis. In fixed IF experiments of mitotic cells the average ratio of MS to untreated H3K9me^{2,3} measurement was 1.6 ± 0.1, whereas the average ratio of MS to untreated H3K27me^{3} measurement was 3.9 ± 0.5 (Figure 3, A and B). In contrast to the fixed IF experiments, MS did not cause a statistically significant change in H3K9me^{2,3} or H3K27me^{3} measurement using antibodies microsprayed onto single captured chromosomes (Figure 3, C and D). Although unexpected, these data are explainable due to a lack of antibody accessibility and penetration into the more compact hypermethylated chromosomes, and the short antibody incubation time for our microspraying of captured chromosomes, relative to fixed IF staining (~10 min vs. ~16 h).

To determine whether increased methylation caused mitotic chromosomes to become stiffer, we measured the doubling force of MS-treated chromosomes. MS treatment caused a statistically significant increase of ~80% in the doubling force of mitotic chromosomes, consistent with more compact chromatin (Figure 3E). The average chromosome doubling forces were 320 ± 30 pN in untreated cells and 580 ± 40 pN in MS-treated cells. This change was not due to a change in either the initial chromosome length or cross-sectional area, as neither changed with MS treatment (Supplemental Figure S3, D and E).

Plotting doubling force against H3K9me^{2,3} measurements did not show any correlation in untreated or MS-treated cells (Supplemental Figure S3F, left panels). Alternately, plotting doubling force against H3K27me^{3} measurements (in MS-treated cells, but not untreated) suggests a potential correlation between H3K27me^{3} and chromosome stiffness (Supplemental Figure S3F, right panels).

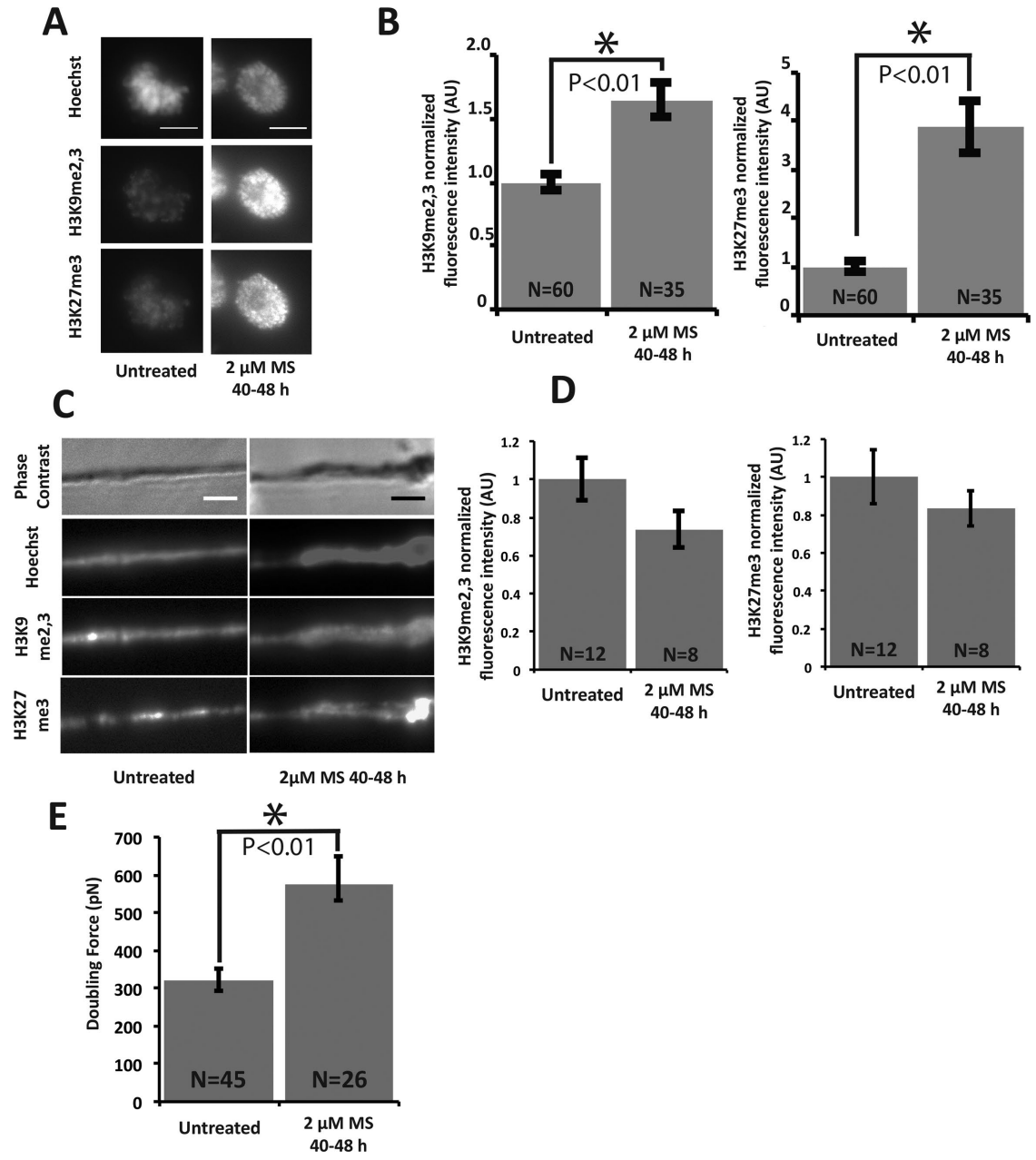

FIGURE 3: Methylstat (HDMi) treatment causes an increase in methylation for mitotic fixed cells and stiffens mitotic chromosomes. (A) Example representative images of levels of H3K9me^{2,3} and H3K27me^{3} fluorescence intensity on fixed mitotic cells. Scale bar = 10 μm. (B) Quantitative data of A. The H3K9me^{2,3} intensity ratio of untreated to 2 μM MS 40–48 h treatment was 1.9 ± 0.1 and is statistically significant. The H3K27me^{3} intensity ratio of untreated to 2 μM MS 40–48 h treatment was 4.4 ± 0.5 and is statistically significant. (C) Example representative images of levels of H3K9me^{2,3} and H3K27me^{3} fluorescence intensity on captured mitotic chromosomes. Scale bar = 5 μm. (D) Quantitative data of C. The H3K9me^{2,3} intensity ratio of untreated to 2 μM MS 40–48 h treatment was 0.73 ± 0.10, statistically insignificantly different from untreated cells. The H3K27me^{3} intensity ratio of untreated to 2 μM MS 40–48 h treatment was 0.81 ± 0.09, statistically insignificantly different from untreated cells. (E) Recorded doubling force for mitotic chromosomes from untreated and MS-treated cells. The average chromosome doubling forces were 320 ± 30 pN in untreated cells. The average doubling force was 580 ± 40 pN in 2 μM MS 40–48 h treated cells, a statistically significant increase of ~80% compared with untreated cells. Error bars represent SE. Asterisk in bar graphs represents a statistically significant difference ($p < 0.05$). All p values were calculated via t test.

However, there may be limitations of antibody accessibility on the chromosomes, so this correlation must be regarded as preliminary at best. Our results do indicate that hypermethylation, via MS treatment, leads to robustly higher H3K27me^{3} levels, and causes chromosomes to become stiffer and possibly denser.

Methylstat treatment does not change SMC2 levels

Because condensin is the most well known contributor to chromosome strength, we sought to check whether levels of condensin on mitotic chromosomes increased when treated with MS. Previous work has shown that chromosome stiffness is approximately linearly

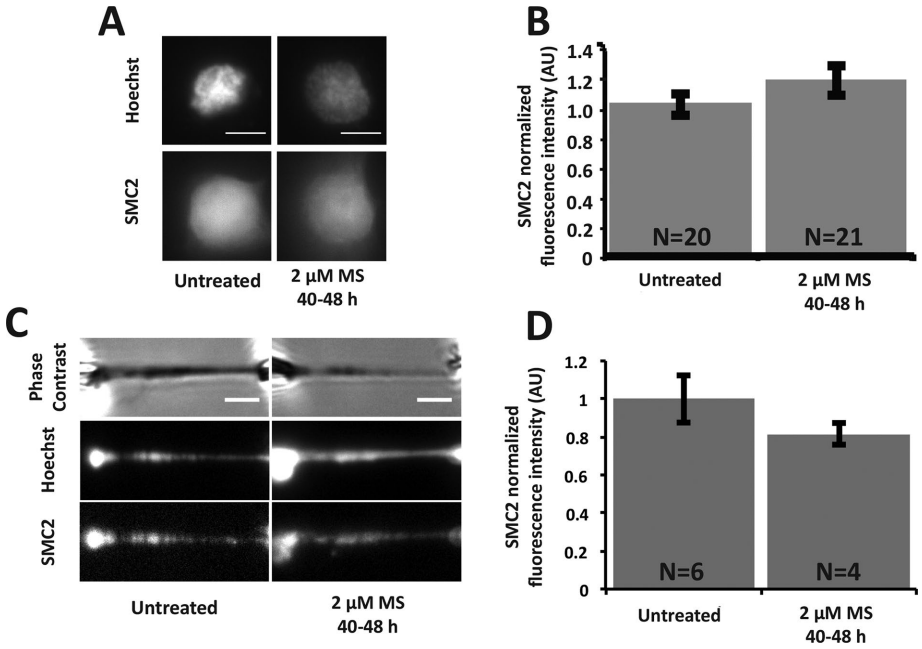

FIGURE 4: Methylstat treatment does not cause a change in SMC2 fluorescence levels. (A) Example representative images of levels of SMC2 fluorescence intensity on fixed mitotic cells. Scale bar = 10 μm. (B) Quantitative data of A. The SMC2 intensity ratio of untreated to 2 μM MS 40–48 h treatment was 1.1 ± 0.1, statistically insignificantly different from untreated cells. (C) Example representative images of levels of SMC2 fluorescence on captured mitotic chromosomes. Scale bar = 5 μm. (D) Quantitative data of C. The SMC2 intensity ratio of untreated to 2 μM MS 40–48 h treatment was 0.82 ± 0.05, statistically insignificantly different. All *p* values calculated via *t* test.

proportional to the amount of condensin on the chromosome (Sun *et al.*, 2018). We used antibodies against SMC2, a core subunit of condensin, to determine whether there was a difference in fluorescence intensities between untreated and MS-treated cells and captured chromosomes. The experiments did not show a difference as measured using fixed cellular immunofluorescence (Figure 4, A and B) or for antibodies microsprayed onto captured chromosomes (Figure 4, C and D), suggesting that the stiffening phenotype is independent of condensin loading.

DISCUSSION

Histone hypermethylation stiffens mitotic chromosomes, but hyperacetylation does not affect mitotic chromosome stiffness

Our data show that increasing histone acetylation (specifically the H3K9ac level) by HDACi treatment does not affect chromosome stiffness in mitosis (Figure 2). Our original hypothesis had been that HDACi-induced histone hyperacetylation would weaken mitotic chromosomes. This hypothesis was based on the observations that histone acetylation is normally reduced in mitosis (Doenecke, 2014), and is thought to intrinsically affect nucleosome packing (Zhiteneva *et al.*, 2017). Furthermore, we expected to see weaker mitotic chromosomes because interphase hyperacetylated chromatin is decompacted (Doenecke, 2014), and hyperacetylating chromatin weakens the chromatin-dependent stiffness of interphase nuclei (Stephens *et al.*, 2017, 2018). However, our data indicate that mitotic chromosomes with hyperacetylated histones via HDACi treatment are overall just as stiff as mitotic chromosomes from untreated cells.

Unlike HDACi treatments, which do not change the doubling force of mitotic chromosomes, treatment by the HDMi MS causes increased histone methylation (assayed via H3K9 and H3K27 methylation) and a stiffer and likely denser mitotic chromosome without affecting SMC2 levels (Figures 3 and 4). These results support our original hypothesis that the increase of histone methylation and propensity of mitotic histones to condense would stiffen mitotic chromosome as observed for interphase nuclei (Stephens *et al.*, 2017, 2018), but contrast with our results involving mitotic hyperacetylated histones. Our data indicate that this stiffening is not due to overloading of condensin, which suggests other mechanisms/complexes may affect chromosomal stiffness.

Incorporating chromatin interactions into the model of mitotic chromosomes

To understand how chromatin may contribute to the overall stiffness of mitotic chromosomes, it is important to understand how mitotic chromosomes are organized. Early electron microscopy suggested that mitotic chromosomes are organized into loops of chromatin extending from a protein-rich core (Marsden and Laemmli, 1979). The currently heavily studied loop-extrusion model builds upon this classical bottlebrush model, describing how the bottlebrush is formed (Alipour and Marko, 2012; Goloborodko *et al.*, 2016; Gibcus *et al.*, 2018). In this model, chromatin loop-extruding complexes in the core of mitotic chromosomes create the bottlebrush structure. Nonhistone chromatin-organizing complexes such as condensin and cohesin localize to the core of mitotic chromosomes and between sister chromatids, respectively (Ball and Yokomori, 2001; Piazza *et al.*, 2013), which according to the model function as loop-extruding enzymes. A broadly similar model of extruded chromatin loops organized by the protein complexes condensin and cohesin has been used to describe the vertebrate and yeast centromere as a chromatin spring (Ribeiro *et al.*, 2009; Stephens *et al.*, 2011; Lawrimore *et al.*, 2015).

We sought to incorporate the loop-extrusion model into the gel-network model of mitotic chromosomes. The gel-network model describes mitotic chromosomes as a gel of chromatin cross-linked by nonhistone protein complexes, predominantly condensin (Figure 5A; Poirier and Marko, 2002). Two facets govern the stiffness of a gel network: the density of cross-links, and the pliability of the intervening cross-linked fibers (de Gennes, 1979). Older work has shown that condensin is responsible for about half of the spring constant of the kintetochore (Ribeiro *et al.*, 2009). Recent work has shown that condensin is approximately linearly correlated to the stiffness of mitotic chromosomes (Sun *et al.*, 2018), suggesting that most of the stiffness is governed by the chromatin loop-extruding elements, which are also apparently the primary cross-linking elements (Figure 5A). Previous work has shown that DNA/chromatin constitutes the underlying connectivity of mitotic chromosomes, which makes up the underlying fiber (Poirier and Marko, 2002; Sun *et al.*, 2011). These data also show that the loop-extruding proteins cannot form a contiguous core. In considering mitotic chromosomes as a gel, condensins comprise the major cross-links whereas chromatin forms the underlying fiber. Both the lack of change in stiffness when histones are hyperacetylated and the lack of increase in condensin

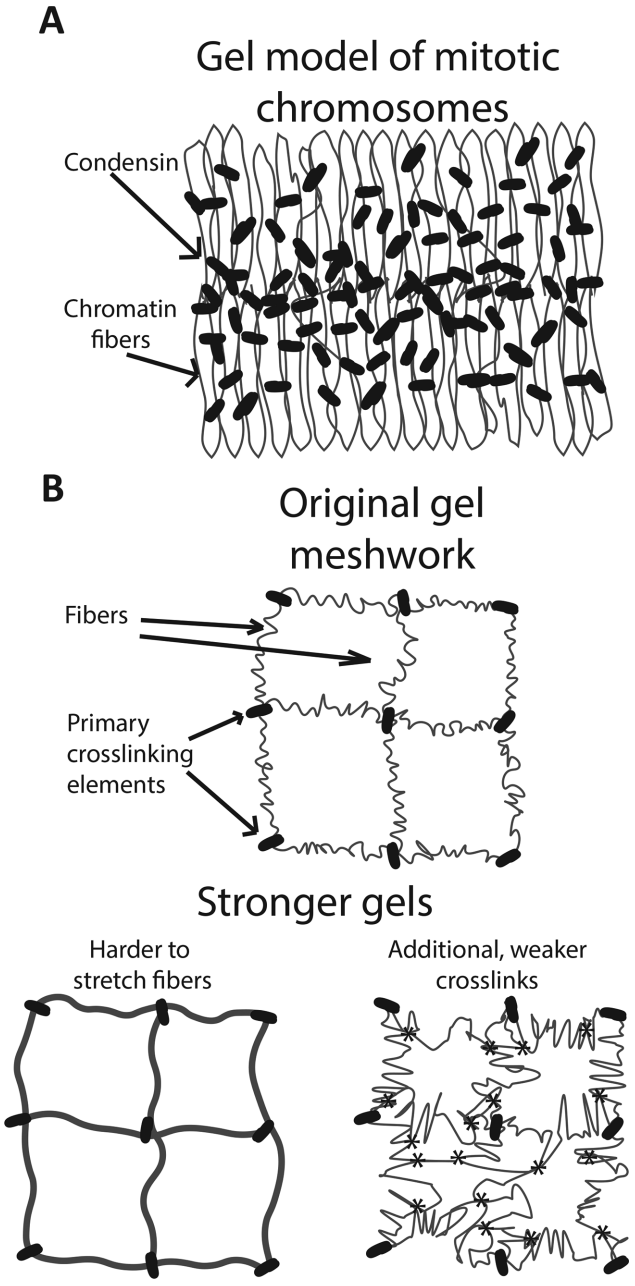

FIGURE 5: Model of mitotic chromosome. (A) Gel-based model of mitotic chromosomes, demonstrating the cross-linking elements as condensin and the intervening fibers as chromatin. This model is compatible with different models of mitotic chromosomes including the loop-extrusion model, in which condensin can act as both a cross-linking element and the loop-extruding element. (B) Methods in which changes to the chromatin fiber or interactions of the chromatin fiber can stiffen a gel network. These models are not mutually exclusive and can be used to describe how increased histone methylation introduces an increase in stiffness to mitotic chromosomes. Neither of these effects is changed when histones are hyperacetylated in mitosis.

levels on hypermethylated histones suggest that perturbing histone PTMs does not affect the number of primary, condensin-based cross-links.

Because hyperacetylation of histones through HDACi treatments does not affect the stiffness of mitotic chromosomes, it cannot affect the number of cross-links or the ability of the chromatin fiber to be stretched. This is in contrast to interphase, in which hyperacetylation weakens chromatin-based nuclear stiffness (Stephens *et al.*, 2017, 2018). This difference may be due to a lack of transcription in mitosis, acetyl-histone readers in mitosis, or other cell-cycle–dependent factors. These factors could actively decompact chromatin in interphase nuclei, but not in mitosis (Wang and Higgins, 2013; Doenecke, 2014). Furthermore, histone acetylation is drastically decreased in mitosis meaning that that the effect of increased histone acetylation via HDACi may be negligible for metaphase chromosomes. Although a decrease in acetylation in mitosis coincides with a higher degree of compaction (Zhiteneva *et al.*, 2017), it appears that the increased acetylation of histones caused by our treatments with HDACis does not have an intrinsic effect on metaphase chromosome stiffness.

Our data suggest that hypermethylation of histones does affect mitotic chromosome structure, given the increased doubling force. Nucleosome–nucleosome interactions can stiffen mitotic chromosomes by either forming additional weaker cross-links or the chromatin fibers themselves could become harder to stretch (Figure 5B). Neither of these hypotheses necessarily affects the primary cross-linkers, condensins. These two hypotheses are not mutually exclusive, although future experiments may be able to determine which of them is predominantly true. Further chromosome-manipulation experiments of the sort presented in this article should be able to determine precisely which PTMs are responsible for the structural changes, as well as elucidate whether the changes in chromosome mechanics we have observed are achieved by histones alone or whether they require other proteins for their mediation.

A majority of work on the relation between histone PTMs and chromatin structure focuses on histone readers, but histone PTMs themselves may be intrinsically responsible for the stiffness change. It has been shown that chromatin reconstituted from mitotic histones aggregates more than chromatin reconstituted from interphase histones (Zhiteneva *et al.*, 2017). This analysis indicates that histone methylation is coupled to the structure and mechanics of mitotic chromosomes, in that a 3.4-fold increase in methylation is associated with an 80% increase in chromosome stiffness. This change in intrinsic condensation tendency may be facilitated by direct nucleosome–nucleosome interactions due to histone tails in the manner observed by (Bilokapic *et al.*, 2018). Our data do suggest that the potential increase of histone methylation, rather than decreased acetylation, contributes to tighter packing of nucleosomes during mitosis.

One must keep in mind that the metaphase chromosome, although organized as a chromatin gel, likely has an underlying radial-loop architecture, with an excess of condensin cross-linkers near the central chromatin "axes" (sketched in Figure 5A). It is conceivable that weak, multivalent attractions between nucleosomes, such as those that might be mediated by methylated histone tails, could drive compaction of the denser axial region of metaphase chromatids without generating adhesion between the outer, less dense outer radial-loop "halos." Uncontrolled adhesion between nucleosomes must be avoided: once individual nucleosomes adhere to one another, the whole genome will stick together and form a droplet, a situation incompatible with chromosome segregation (Marko and Siggia, 1997). Multivalency could be a key ingredient, as it can permit a rapid "turn on" of internucleosome attraction with local nucleosome concentration, allowing the relatively weak loop-extrusion compaction by condensins to compact the axial region sufficiently so that attractions turn on there, but not in the less dense loop halo. This scenario could explain how metaphase chromatids

end up being dense in their axial interior while retaining mutually repulsive loop-halo exteriors, thus simultaneously achieving strong chromatin compaction while facilitating chromosome individualization and sister chromatid resolution, and also making the overall mechanics of metaphase chromosomes sensitive to additional nucleosome attractions associated with specific PTMs.

MATERIALS AND METHODS

Cell culture and drug treatments

Human HeLa cells were maintained in DMEM (Corning) with 10% fetal bovine serum (FBS; HyClone) and 1% 100× penicillin/streptomycin (Corning). The cells were incubated at 37°C and 5% CO_2 for no more than 30 generations, and were passaged every 2–4 d. Experiments on captured chromosomes used cells that were allowed to recover 1–3 d before capture. Cells were freely cycling and not treated with drugs designed to affect or synchronize the cell cycle.

For epigenetic drug treatments, the cells were plated as above in drug-free DMEM and allowed to recover for ~8 h, and then treated with 2 mM VPA (Sigma), 50 nM TSA (Sigma), or 2 μM MS (Cayman Chemicals), all dissolved in DMEM. Chromosomes were then captured from the cells (see below) 16–24 h after treatment for VPA and TSA, or 40–48 h for MS treatments.

Fixed IF

Cells were grown in small wells built on coverslips (Fisher) and treated as above. All solutions were diluted with and wash steps performed with PBS (Lonza) at room temperature, unless noted otherwise. Slides were washed, fixed in 4% paraformaldehyde (EMS), washed, permeabilized with 0.10–0.20% Triton X-100 (USBio), incubated in 0.06% Tween 20 (Fisher), washed, and blocked in 10% goat serum (Sigma). The slides were incubated with a primary solution overnight at 4°C. The slides were then washed, incubated in a secondary solution, incubated in Hoechst (Life Tech), washed, and mounted.

Primary and secondary solutions were diluted in 10% goat serum. HDACi treatments were assayed using a 1:400 rabbit anti-H3K9ac (Cell Signaling; 9649) primary solution and a 1:500 488-nm anti-rabbit immunoglobulin G (IgG) (Invitrogen; A11034) secondary solution. HDMi treatments used 1:100 mouse anti-H3K9me^{2,3} (Cell Signaling; 5327) with1:1600 rabbit anti-H3K27me^{3} (Cell Signaling; 9733) primary solution and 1:500 of 488-nm anti-mouse IgG (Invitrogen; A11001) with 1:500 of 594-nm anti-rabbit IgG (Invitrogen; A11037) secondary solution. Mitotic cells were identified by finding cells that showed compact mitotic chromosomes in the Hoechst channel. The final IF values reported are given by the fluorescence signal to background ratio of the antibody of interest over the Hoechst signal to background ratio. Averages and standard errors are divided by the average untreated values in normalized graphs.

Single chromosome capture: setup and microscopy

Single chromosome capture experiments used an inverted microscope (IX-70; Olympus) with a 60× 1.42 NA oil immersion objective with a 1.5× magnification pullout at room temperature and atmospheric CO_2 levels. Experiments were performed in less than 3 h after removal from the incubator to ensure minimum damage to the cells being analyzed.

Prometaphase cells were identified by eye and lysed with 0.05% Triton X-100 in PBS. All other pipettes were filled with PBS. After lysis, the bundle of chromosomes was held with a pipette. One end of a random, loose chromosome was grabbed by the force pipette (WPI TW100F-6), moved from the bundle, and grabbed with the pulling pipette on the other end. The bundle was then removed to isolate the tracked and unbroken chromosome (Figure 1A and Supplemental Figure S1).

Single chromosome capture: force measurement

An easily bendable force pipette and stiff pulling pipette were used for stretching chromosomes. Once captured, the pipettes were moved perpendicular to the chromosome, stretching the chromosome to roughly its native length. The stiff pipette was then moved 6 μm and returned to the starting position at a constant rate of 0.20 μm/s in 0.04 μm steps using a LabVIEW program, while tracking the stiff and force pipette. Figure 1B shows an example stretch-deflection experiment. Deflection of the force pipette multiplied by its calibrated spring constant and divided by the distance between the pipettes (the stretch) was used to obtain the chromosome spring constant. Each chromosome was stretched at least three times to provide an accurate and reproducible measurement of the chromosome spring constant. The chromosome spring constant multiplied by its initial length gave the doubling force. The initial length was given by measuring the distance between the centers of the pipettes in ImageJ and converting the pixels into microns while the chromosome was perpendicular to the pipettes. The chromosome cross-sectional area was estimated as $0.25\pi d^2$ with the chromosome diameter d calculated as the full width at half maximum of an ImageJ line scan.

Single chromosome capture: immunofluorescence

After force measurements, the chromosome was lifted above the glass surface and microsprayed with a primary, secondary, and tertiary solution from a wide bore pipette, moving the chromosome between sprays. The solutions used 50 μl PBS, 36–38 μl USP sterile molecular biology grade water (Corning), 10 μl 5% casein (Sigma), and 2 μl of each antibody. HDACi experiments used a rabbit anti-H3K9ac primary solution and a 488-nm anti-rabbit secondary solution. HDMi experiments used a mouse anti-H3K9me^{2,3} and a rabbit anti-H3K27me^{3} primary solution and a 488-nm anti-mouse IgG with a 594-nm anti-rabbit IgG secondary solution. The tertiary spray used Hoechst instead of an antibody.

Western blots

Cells were grown in 100-mm dishes and treated as described in *Cell culture and treatments*. TSA treatments were done at 200 nM. Cells were then harvested in PBS, centrifuged into a pellet, and lysed with RIPA buffer. The solution was then pelleted and the supernatant saved. The solution was then mixed with 2× Laemmli buffer, run on a 4–20% gradient SDS–PAGE gel, transferred to a nitrocellulose sheet, incubated in a primary solution, washed, and incubated in a secondary solution, then imaged.

Statistics

For fixed immunofluorescence, the reported N refers to the number of technical replicates, that is, the total number of cells analyzed. The N measurements are furthermore from a set of biological replicates, that is, separate cell colonies on separate slides. All interphase-staining results are from data taken from two biological replicates. Mitotic staining for H3K9ac and SMC2 was also obtained using two biological replicates. H3K9me^{2,3} and H3K27me^{3} data came from four biological replicates. For captured chromosomes, the reported N refers to each individual captured chromosome for both mechanical and immunofluorescence experiments; these experiments were from different slides (colonies) of cells and thus are independent biological replicates. Outliers were identified and

discarded by using a generalized Studentized deviate test at $\alpha = 0.05$. All p values were calculated using a t test. All averaged values are reported as average ± SE.

ACKNOWLEDGMENTS

This work was supported by the National Institutes of Health through Grants no. R01-GM105847, U54-CA193419 (CR-PS-OC), by a subcontract to Grant U54-DK107980 (4DN), and by Grant K99-GM123195 (A.D.S.).

REFERENCES

Alipour E, Marko JF (2012). Self-organization of domain structures by DNA-loop-extruding enzymes. Nucleic Acids Res 40, 11202–11212.

Ball AR Jr, Yokomori K (2001). The structural maintenance of chromosomes (SMC) family of proteins in mammals. Chromosome Res 9, 85–96.

Banigan EJ, Stephens AD, Marko JF (2017). Mechanics and buckling of biopolymeric shells and cell nuclei. Biophys J 113, 1654–1663.

Beck DB, Oda H, Shen SS, Reinberg D (2012). PR-Set7 and H4K20me1: at the crossroads of genome integrity, cell cycle, chromosome condensation, and transcription. Genes Dev 26, 325–337.

Bilokapic S, Strauss M, Halic M (2018). Cryo-EM of nucleosome core particle interactions in trans. Sci Rep 8, 7046.

Chalut KJ, Hopfler M, Lautenschlager F, Boyde L, Chan CJ, Ekpenyong A, Martinez-Arias A, Guck J (2012). Chromatin decondensation and nuclear softening accompany Nanog downregulation in embryonic stem cells. Biophys J 103, 2060–2070.

Chow KH, Factor RE, Ullman KS (2012). The nuclear envelope environment and its cancer connections. Nat Rev Cancer 12, 196–209.

de Gennes PG (1979). Scaling Concepts in Polymer Physics, Ithaca, NY: Cornell University Press.

Doenecke D (2014). Chromatin dynamics from S-phase to mitosis: contributions of histone modifications. Cell Tissue Res 356, 467–475.

Gibcus JH, Samejima K, Goloborodko A, Samejima I, Naumova N, Nuebler J, Kanemaki MT, Xie L, Paulson JR, Earnshaw WC, *et al.* (2018). A pathway for mitotic chromosome formation. Science 359, eaao6135.

Goloborodko A, Imakaev MV, Marko JF, Mirny L (2016). Compaction and segregation of sister chromatids via active loop extrusion. Elife 5, e14864.

Haase K, Macadangdang JK, Edrington CH, Cuerrier CM, Hadjiantoniou S, Harden JL, Skerjanc IS, Pelling AE (2016). Extracellular forces cause the nucleus to deform in a highly controlled anisotropic manner. Sci Rep 6, 21300.

Krause M, Te Riet J, Wolf K (2013). Probing the compressibility of tumor cell nuclei by combined atomic force-confocal microscopy. Phys Biol 10, 065002.

Lawrimore J, Vasquez PA, Falvo MR, Taylor RM 2nd, Vicci L, Yeh E, Forest MG, Bloom K (2015). DNA loops generate intracentromere tension in mitosis. J Cell Biol 210, 553–564.

Luo X, Liu Y, Kubicek S, Myllyharju J, Tumber A, Ng S, Che KH, Podoll J, Heightman TD, Oppermann U, *et al.* (2011). A selective inhibitor and probe of the cellular functions of Jumonji C domain-containing histone demethylases. J Am Chem Soc 133, 9451–9456.

Marchion DC, Bicaku E, Daud AI, Sullivan DM, Munster PN (2005). Valproic acid alters chromatin structure by regulation of chromatin modulation proteins. Cancer Res 65, 3815–3822.

Marko JF, Siggia ED (1997). Polymer models of meiotic and mitotic chromosomes. Mol Biol Cell 8, 2217–2231.

Marsden MP, Laemmli UK (1979). Metaphase chromosome structure: evidence for a radial loop model. Cell 17, 849–858.

Oomen ME, Dekker J (2017). Epigenetic characteristics of the mitotic chromosome in 1D and 3D. Crit Rev Biochem Mol Biol 52, 185–204.

Park JA, Kim AJ, Kang Y, Jung YJ, Kim HK, Kim KC (2011). Deacetylation and methylation at histone H3 lysine 9 (H3K9) coordinate chromosome condensation during cell cycle progression. Mol Cells 31, 343–349.

Piazza I, Haering CH, Rutkowska A (2013). Condensin: crafting the chromosome landscape. Chromosoma 122, 175–190.

Poirier MG, Marko JF (2002). Mitotic chromosomes are chromatin networks without a mechanically contiguous protein scaffold. Proc Natl Acad Sci USA 99, 15393–15397.

Ribeiro SA, Gatlin JC, Dong Y, Joglekar A, Cameron L, Hudson DF, Farr CJ, McEwen BF, Salmon ED, Earnshaw WC, Vagnarelli P (2009). Condensin regulates the stiffness of vertebrate centromeres. Mol Biol Cell 20, 2371–2380.

Rice JC, Allis CD (2001). Histone methylation versus histone acetylation: new insights into epigenetic regulation. Curr Opin Cell Biol 13, 263–273.

Stephens AD, Banigan EJ, Adam SA, Goldman RD, Marko JF (2017). Chromatin and lamin A determine two different mechanical response regimes of the cell nucleus. Mol Biol Cell 28, 1984–1996.

Stephens AD, Haase J, Vicci L, Taylor RM 2nd, Bloom K (2011). Cohesin, condensin, and the intramolecular centromere loop together generate the mitotic chromatin spring. J Cell Biol 193, 1167–1180.

Stephens AD, Liu PZ, Banigan EJ, Almassalha LM, Backman V, Adam SA, Goldman RD, Marko JF (2018). Chromatin histone modifications and rigidity affect nuclear morphology independent of lamins. Mol Biol Cell 29, 220–233.

Sun M, Biggs R, Hornick J, Marko JF (2018). Condensin controls mitotic chromosome stiffness and stability without forming a structurally contiguous scaffold. Chromosome Res 26, 277–295.

Sun M, Kawamura R, Marko JF (2011). Micromechanics of human mitotic chromosomes. Phys Biol 8, 015003.

Vagnarelli P (2012). Mitotic chromosome condensation in vertebrates. Exp Cell Res 318, 1435–1441.

Walther N, Hossain MJ, Politi AZ, Koch B, Kueblbeck M, Odegard-Fougner O, Lampe M, Ellenberg J (2018). A quantitative map of human condensins provides new insights into mitotic chromosome architecture. J Cell Biol 217, 2309–2328.

Wang F, Higgins JM (2013). Histone modifications and mitosis: countermarks, landmarks, and bookmarks. Trends Cell Biol 23, 175–184.

Xu D, Bai J, Duan Q, Costa M, Dai W (2009). Covalent modifications of histones during mitosis and meiosis. Cell Cycle 8, 3688–3694.

Yoshida M, Kijima M, Akita M, Beppu T (1990). Potent and specific inhibition of mammalian histone deacetylase both in vivo and in vitro by trichostatin A. J Biol Chem 265, 17174–17179.

Zhiteneva A, Bonfiglio JJ, Makarov A, Colby T, Vagnarelli P, Schirmer EC, Matic I, Earnshaw WC (2017). Mitotic post-translational modifications of histones promote chromatin compaction in vitro. Open Biol 7, e170076.